

Cite this: *Chem. Sci.*, 2014, 5, 4610

## Antiparallel three-component gradients in double-channel surface architectures†

Hironobu Hayashi,‡ Adam Sobczuk, Altan Bolag, Naomi Sakai and Stefan Matile\*

The synthesis of multicomponent surface architectures with a thus far inaccessible level of sophistication is accomplished, and the functional relevance of this unprecedented structural complexity is demonstrated. Co-axial channels of oligothiophenes and fullerenes for the transport of holes and electrons, respectively, are equipped with antiparallel-oriented redox gradients with up to three components that drive the charges apart after their generation with light. In the resulting photosystems, charge recombination decreases with each level of sophistication from 29% to 2%, approaching complete suppression. Photocurrents increase correspondingly, and thermal activation barriers decrease. Increasing turn-on voltages for dark current indicates that charges struggle to move backwards up gradients possessing increasing numbers of components. These results demonstrate that the application of the most complex lessons from nature to organic materials is possible and worthwhile, thus supporting curiosity-driven efforts to learn how to synthesize multicomponent architectures of the highest possible sophistication with the highest possible precision.

Received 15th July 2014  
Accepted 28th August 2014

DOI: 10.1039/c4sc02092h

www.rsc.org/chemicalscience

Significant biological functions are often accomplished using supramolecular architectures of overwhelming complexity.<sup>1</sup> No one knows what we would obtain from organic materials of comparable sophistication because the methods for their synthesis remain rudimentary despite significant efforts worldwide.<sup>1–17</sup> Particularly challenging is synthetic control over the directionality of multicomponent architectures. However, this directionality is of scientific interest for many reasons. In biological photosystems, for example, electrons and holes, after their generation with light, are guided in opposite directions along oriented multicomponent redox gradients in separate charge-transport pathways.<sup>1</sup> While molecular systems with co-axial hole (h<sup>+</sup>) and electron (e<sup>−</sup>) transporting channels have been synthesized,<sup>1–21</sup> the installation of antiparallel-oriented multicomponent gradients in these co-axial channels remains difficult because it requires directionality.<sup>1</sup> To contribute towards synthetic methods that control directionality in multicomponent architectures, we have introduced zipper assembly<sup>22</sup> and self-organizing surface-initiated polymerization (SOSIP).<sup>23</sup> Robust and user-friendly, SOSIP has been further expanded to include templated self-sorting (TSS)<sup>24</sup> and templated stack exchange (TSE).<sup>25</sup> Here, we use SOSIP-TSE to synthesize the first double-channel architecture with antiparallel-oriented redox

gradients composed of three components each, and show that this [3 + 3] architecture, as sophisticated as it gets today, is functionally relevant.

The complete series of [1 + 1] photosystem 1 with co-axial channels but without gradients, [2 + 2] photosystem 2 with antiparallel gradients composed of two components each, and the ultimate “triple-gradient” [3 + 3] photosystem 3 was designed as follows (Fig. 1). Oligothiophenes<sup>26</sup> and fullerenes<sup>27</sup> were selected as hole and electron transporters, respectively. For gradients in the p-channel, we envisioned raising and lowering the HOMO energy of quaterthiophenes (TT)<sup>13,26</sup> with two ethylenedioxythiophenes (TE)<sup>13,28,29</sup> and two thiazoles (TA)<sup>13,30,31</sup> in the middle of the tetramer, respectively. In the n-channel, the LUMO level of Bingel fullerenes (SB) has been shown to gradually rise in double-Bingel fullerenes (DB) and double-Bingel methanofullerenes (DM).<sup>7,15,16,27</sup> Architectures used for control experiments included the gradient-free single-channel [1 + 0] photosystem 4.

The components 5–11 were further equipped with all that is needed for SOSIP-TSE (Fig. 1, 2 and S1†).<sup>25</sup> Added to both termini of the TA oligomer in 5 were (i) two diphosphonate “feet” to bind to the indium tin oxide (ITO) surface, (ii) a naphthalenediimide (NDI) to template for TSE and (iii) a protected cysteine to initiate disulfide-exchange polymerization (Fig. 2A). The termini of TA, TT and TE oligomers in 6–8 all contain (i) a benzaldehyde-protected hydrazide for TSE and (ii) a strained cyclic disulfide from asparagusic acid to propagate the ring-opening disulfide-exchange polymerization initiated by 5 (Fig. 2A). The fullerene stack exchangers 9–11 were equipped with an aldehyde and two triethyleneglycol chains to assure

Department of Organic Chemistry, University of Geneva, Geneva, Switzerland. E-mail: stefan.matile@unige.ch; Web: <http://www.unige.ch/sciences/chiorg/matile/>; Fax: +41 22 379 5123; Tel: +41 22 379 6523

† Electronic supplementary information (ESI) available: Detailed procedures and results for all reported experiments. See DOI: 10.1039/c4sc02092h

‡ Present address: Graduate School of Materials Science, Nara Institute of Science and Technology (NAIST), Nara, Japan.

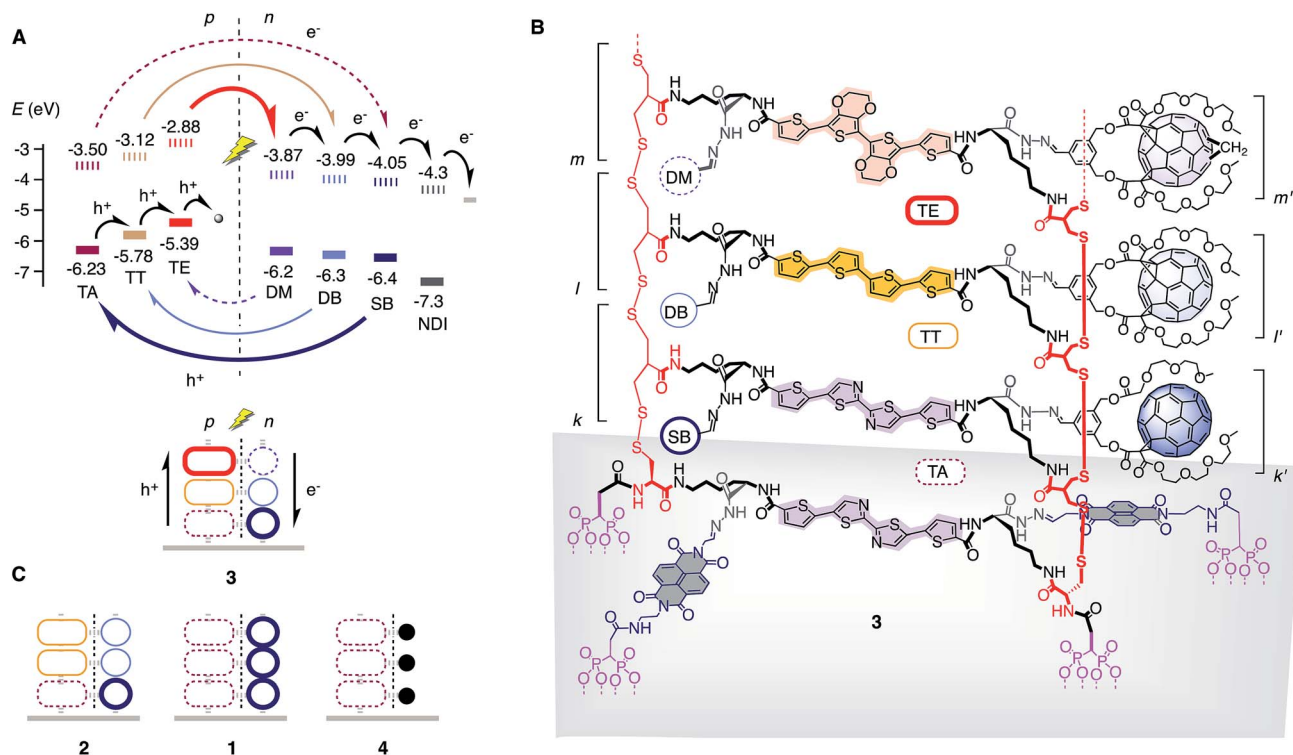


Fig. 1 Design of antiparallel three-component gradients. (A) Schematic structure of photosystem 3 with HOMO (bold) and LUMO (dashed) energy levels (from differential pulse voltammetry, normalized against  $-5.1$  eV for  $\text{Fc}^+/\text{Fc}$ , see Fig. S3 and Table S1;† shaded circles and grey line indicate ascorbic acid and ITO as final acceptors, respectively), and with hole ( $\text{h}^+$ ) and electron ( $\text{e}^-$ ) transfer cascades for photoinduced charge separation and translocation in p- and n-transporting channels, respectively. (B) Molecular structure of photosystem 3. (C) Schematic structure of control systems 1, 2 and 4 (● = hydrazone from benzaldehyde, compare with 6). The structures shown are consistent with design, synthesis and results. However, they are idealized structures; defects will be repaired due to the dynamic covalent chemistry employed, but only to a certain extent.<sup>24,42</sup>

solubility in polar aprotic solvents for TSE (Fig. 1B, 2A and S1†).<sup>27</sup>

The preparation of components 5–11 required substantial multistep synthesis (Schemes S1–S3†). Detailed procedures and analytical data of all new compounds are provided in the ESI.† The HOMO and LUMO energies of the new TA and TE tetramers 6 and 8 were determined by differential pulse voltammetry and optical bandgaps, and were found to be compatible with the construction of antiparallel three-component gradients (Fig. 1A, S2 and S3, Table S1†).

The synthesis of [3 + 3] photosystem 3 began with the deposition of initiator 5 on ITO (Fig. 2A, Schemes S4–S5†). The monolayer was characterized as described for previous systems (Fig. S4†), and the thiols were deprotected on the surface with DTT. For SOSIP, the activated monolayer 12 was incubated in solutions of TA propagator 6 under carefully optimized conditions (Fig. 2A, B and S5, Table S2†). At sufficient thickness (judged from the absorption spectra, Fig. 2B), the obtained [1 + 0] photosystem 13 was incubated with TT propagator 7 to give [2 + 0] photosystem 14, which in turn was incubated with TE propagator 8 to SOSIP the third component of the oriented gradient in [3 + 0] photosystem 15 (Fig. 2A, B and S6†). In all experiments, the oligothiophene absorption maximum at 435 nm of the final [3 + 0] photosystem 15 was set

at  $A \sim 0.3$ – $0.5$  (Fig. 2B). For an ideal  $\pi$ -stack with  $3.4$  Å repeats, this corresponds to a thickness of 100–160 nm ( $\epsilon_{\text{max}} \sim 4.3 \times 10^4 \text{ M}^{-1} \text{ cm}^{-1}$ , Table S1†).

For TSE, the benzaldehyde templates in 15 were removed with excess hydroxylamine, and the large pores in 16 with reactive hydrazides along their walls were filled by reversible hydrazone formation with SB fullerene 9 (Fig. 2A, D and S7†). Part of the fullerene stack in [3 + 1] double-channel photosystem 17 was removed by controlled incubation with hydroxylamine, and the pores in photosystem 18 were filled with DB fullerene 10 (Fig. 2A, C, D and S8†). Removal of part of the fullerenes in [3 + 2] photosystem 19 with hydroxylamine followed by incubation with DM fullerene 11 to fill the shallow pores in 20 gave the [3 + 3] photosystem 3 (Fig. 2D, S9†). The yield of each TSE reaction was determined from changes in the absorption spectra of the transparent electrodes and conditions were systematically optimized until  $>50\%$  was reached (Fig. 2C, D and S7–S11, Table S3†). The control photosystems 1, 2 and 4 were prepared correspondingly.

Photocurrent generation was measured under routine conditions with the photosystems as working electrodes, a platinum wire as a counter electrode and ascorbic acid as a mobile hole transporter in solution (mobile hole transporters other than ascorbic acid were tested as well; triethanolamine

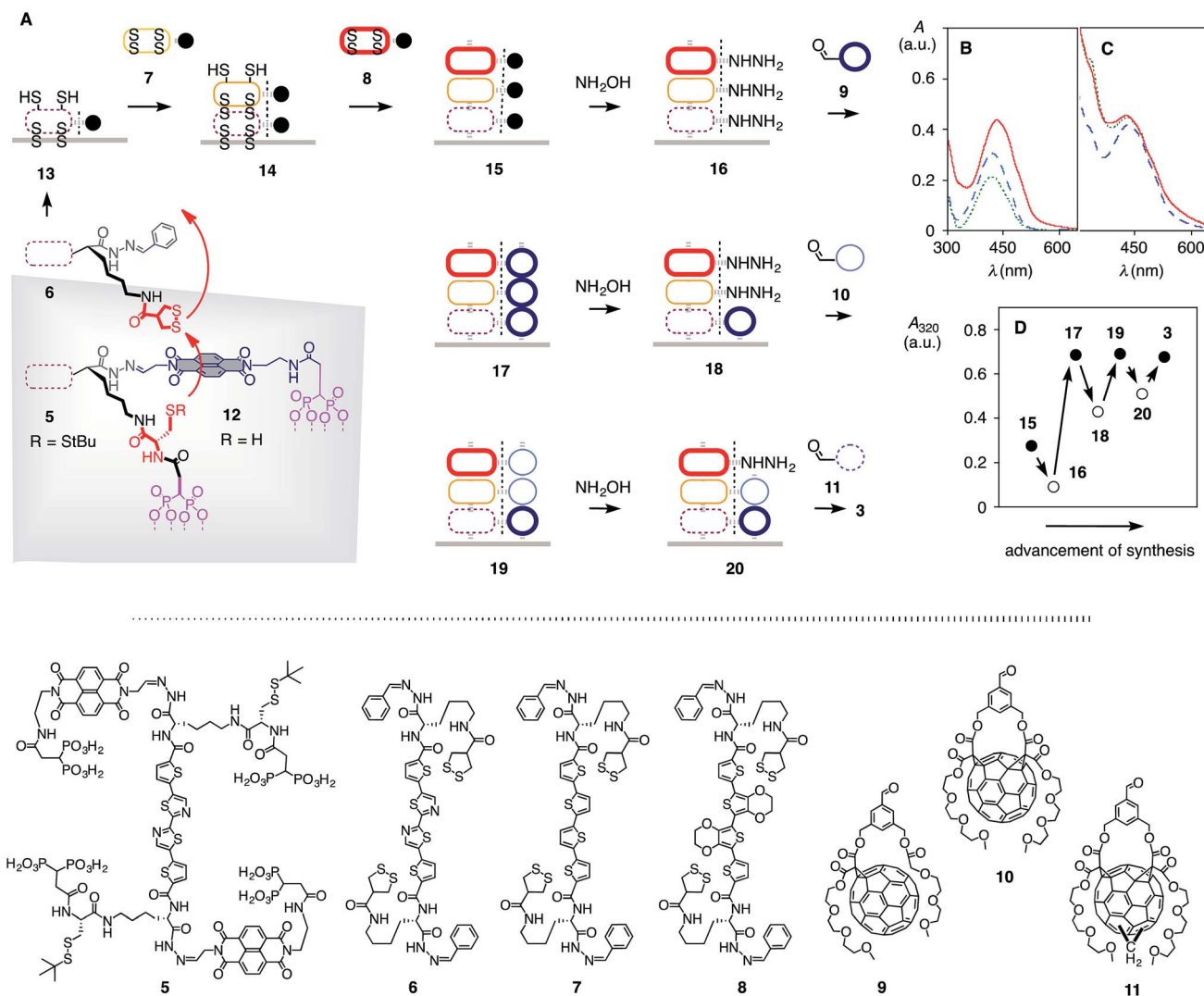


Fig. 2 Synthesis of antiparallel three-component gradients. (A) Synthetic scheme for [3 + 3] architecture 3 (see Fig. 1 and S5–S9† for full structures). (B) Absorption spectra of [1 + 0] architecture 13 (dotted), [2 + 0] 14 (dashed) and [3 + 0] 15 (solid). (C) Absorption spectra of [3 + 1] architecture 17 (dotted), intermediate 18 (dashed) and [3 + 2] 19 (solid). (D) Changes in absorption at 320 nm during TSE (compare Fig. 1 for structures).

gave clearly higher initial photocurrents but seemed to damage the surface of photosystem 3). Results obtained under these conditions are not comparable with those from optimized optoelectronic devices but they are fully appropriate for the evaluation and comparison between different multicomponent architectures.

Triple-gradient photosystem 3 generated clearly more short-circuit photocurrent density  $J_{SC}$  than double-gradient photosystem 2 (Fig. 3A, ● vs. △, Table 1). The [2 + 2] photosystem 2 was in turn more active than the gradient-free [1 + 1] photosystem 1 (Fig. 3A, △ vs. ○), which in turn was much more active than the single-channel [1 + 0] control 4 (Fig. 3A, ○ vs. ◆). These gradual improvements demonstrated that each level of sophistication contributes to the activity of [3 + 3] photosystem 3. The final triple-gradient double-channel photosystem 3 generated about 50-times more  $J_{SC}$  than the simplest [1 + 0] control 4.

The quite remarkable increase of photoactivity from increasing the number of components in the antiparallel oriented gradients could in part be rationalized by the decreasing charge recombination efficiency  $\eta_{BR}$  (Fig. 3B, Table 1). Namely, the dependence of  $J_{SC}$  on the irradiation intensity  $I^{32}$  revealed nearly perfect  $\eta_{BR} = 2\%$  for [3 + 3] photosystem 3 (Fig. 3B, ●), slightly higher  $\eta_{BR} = 19\%$  for [2 + 2] photosystem 2 (Fig. 3B, △) and even higher  $\eta_{BR} = 29\%$  for [1 + 1] photosystem 1 (Fig. 3B, ○). The more pronounced reduction in charge recombination from [2 + 2] to [3 + 3] photosystems, in comparison to the reduction from [1 + 1] to [2 + 2] photosystems, supported the significance of the third component in the gradient.

Increasing charge mobility through increasing complexity was further implied by the temperature dependence of photocurrent  $J_{SC}$  (Fig. 3C).<sup>33–35</sup> According to the Arrhenius plots, the activation energy  $E_a$  needed for photocurrent generation

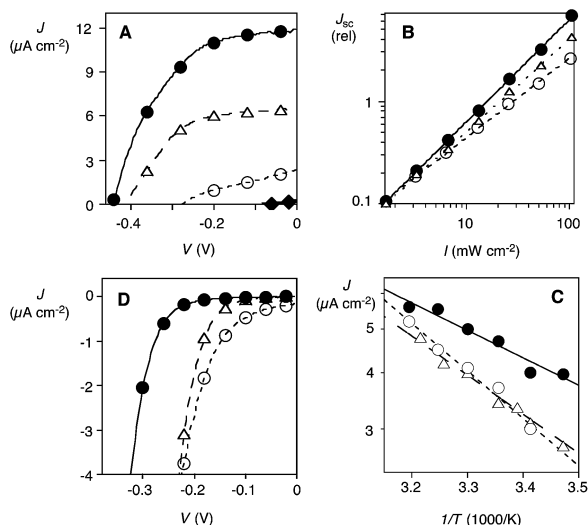


**Fig. 3** Evaluation of antiparallel three-component gradients. (A) Dependence of photocurrent density  $J$  on voltage  $V$  (solar simulator,  $W = 100 \text{ mW}$ ,  $50 \text{ mM}$  ascorbic acid,  $100 \text{ mM}$   $\text{Na}_2\text{SO}_4$ , Pt counter electrode) for **3** ( $\bullet$ ), **2** ( $\Delta$ ), **1** ( $\circ$ ) and **4** ( $\blacklozenge$ ). (B) Dependence of short-circuit photocurrent density  $J_{sc}$  on the irradiation intensity  $I$  for **3** ( $\bullet$ ), **2** ( $\Delta$ ) and **1** ( $\circ$ ) (normalized to  $J_{sc} = 0.1 \mu\text{A cm}^{-2}$  at  $I = 1.63 \text{ mW cm}^{-2}$  to facilitate comparison). (C) Arrhenius plot of  $J_{sc}$  on temperature  $T$  for **3** ( $\bullet$ ), **2** ( $\Delta$ ) and **1** ( $\circ$ ). (D) Dependence of the dark current density  $J$  on voltage  $V$  for **3** ( $\bullet$ ), **2** ( $\Delta$ ) and **1** ( $\circ$ ).

**Table 1** Characteristics of double-channel photosystems with or without antiparallel gradients containing  $[n + m]$  components

PS <sup>a</sup>	$J_{sc}^b$ ( $\mu\text{A cm}^{-2}$ )	$\eta_{BR}^c$ (%)	$E_a^d$ (meV)	$n^e$	$V_d^f$ (mV)
<b>1</b> [1 + 1]	2	29	209	2.58	−130
<b>2</b> [2 + 2]	6	19	172	1.71	−190
<b>3</b> [3 + 3]	12	2	121	1.48	−290

<sup>a</sup> Double-channel photosystems with  $[3 + 3] = \text{triple gradient}$ ,  $[2 + 2] = \text{double gradient}$  and  $[1 + 1] = \text{without gradient}$ , see Fig. 1 for structures.

<sup>b</sup> Short-circuit photocurrent density  $J_{sc}$  generated by irradiation with white light (Fig. 3A). <sup>c</sup> Bimolecular charge recombination efficiencies  $\eta_{BR}$  from the dependence of  $J_{sc}$  on irradiation intensity (Fig. 3B).

<sup>d</sup> Activation energy  $E_a$  from the dependence of  $J_{sc}$  on temperature (Fig. 3C). <sup>e</sup> Ideality factor  $n$ . <sup>f</sup> Turn-on voltage  $V_d$  from the voltage dependence of the dark current (Fig. 3D).

decreased with the increasing sophistication of the charge-transfer cascades, down to  $E_a = 121 \text{ meV}$  for  $[3 + 3]$  photosystem **3** (Table 1). Once again, the addition of the third components significantly affected  $E_a$ .

Dark current measurements were of interest in exploring the characteristics of antiparallel charge-transfer cascades for diode function. The voltage needed to force charges to flow against the direction of the redox gradient is referred to as the turn-on voltage  $V_d$ . The turn-on voltage of the dark current increased with increasing sophistication of the charge-transfer cascade from  $V_d = -130 \text{ mV}$  for gradient-free double-channel  $[1 + 1]$  photosystem **1** to  $V_d = -290 \text{ mV}$  for triple-gradient  $[3 + 3]$  photosystem **3** (Fig. 3D, Table 1). This result confirmed that uphill charge flow becomes harder with more components

contributing to the gradient, and that the contribution of the third component to the gradient is of decisive importance. The significant dependence of turn-on voltage  $V_d$  on the sophistication of the antiparallel gradients naturally also very positively influences the open circuit voltage  $V_{OC}$  of the photocurrents (Fig. 3A).

From the exponential increase of the dark current density  $J$  around the turn-on voltage, formal ideality factors  $n$  were determined.<sup>36,37</sup> Decreasing ideality factors with increasing number of components in the redox gradient confirmed that the lessons learned from  $\eta_{BR}$  and  $E_a$  for photocurrents apply also for dark currents (Fig. 3D, Table 1). Namely, each component added to antiparallel charge-transfer cascades helps to minimize charge trapping and recombination.

Note that most analytical methods used here to quantify the results have been developed in the context of different configurations. Although consistent and comparable within the reported series, the obtained values should not be compared with those obtained with different configurations, and their meaning should be considered with appropriate caution.

Taken together, functional analysis reveals that each level of sophistication engineered into multicomponent architectures improves all aspects of their activity consistently and significantly. Photocurrents increase steadily from the addition of a second co-axial channel, past the introduction of redox gradients composed of two components, to the final three-component charge-transfer cascades in both channels. As in the natural photosystems, charge recombination decreases toward perfection with increasing sophistication of the antiparallel gradients, driving holes and electrons apart right after their generation with light. Thermal activation energies and ideality factors decrease correspondingly, whereas the turn-on voltages for uphill charge movement increase with increasing sophistication of the gradients.

Finally, we would like to highlight the synthetic aspect of this work. Compared to the high standards for small molecules, the synthetic organic chemistry of large systems is poorly developed. To help improve on this situation, we have introduced SOSIP,<sup>23</sup> TSS<sup>24</sup> and TSE<sup>25</sup> as general synthetic methods. The important achievements<sup>1</sup> reported herein demonstrate that these new methods provide synthetic access to the application of one of the most complex lessons from nature to organic materials, *i.e.*, oriented antiparallel three-component gradients. The key to success was the directional use of orthogonal dynamic covalent bonds,<sup>38–41</sup> *i.e.*, disulfide exchange for SOSIP<sup>23</sup> and hydrazone exchange for TSE,<sup>25</sup> in combination with molecular recognition, self-sorting<sup>24</sup> and self-repair.<sup>42</sup> The development of analytical methods to characterize multicomponent architectures at this level of complexity beyond functional feedback loops emerges as a challenge for the future. The results from functional analysis demonstrate that these synthetic efforts towards learning how to construct functional systems of the highest sophistication are worthwhile and are thus expected to stimulate progress in the field in the broadest sense.





## Acknowledgements

We thank the NMR and the Sciences Mass Spectrometry (SMS) platforms for services, and the University of Geneva, the European Research Council (ERC Advanced Investigator), the National Centre of Competence in Research (NCCR) Chemical Biology, the NCCR Molecular Systems Engineering and the Swiss NSF for financial support.

## References

- 1 R. Bhosale, N. Sakai, J. Mísek and S. Matile, *Chem. Soc. Rev.*, 2010, **39**, 138–149, and references therein.
- 2 F. Würthner, *Science*, 2006, **314**, 1693–1694.
- 3 D. M. Bassani, L. Jonusauskaite, A. Lavie-Cambot, N. D. McClenaghan, J.-L. Pozzo, D. Ray and G. Vives, *Coord. Chem. Rev.*, 2010, **254**, 2429–2445.
- 4 T. Marangoni and D. Bonifazi, *Nanoscale*, 2013, **5**, 8837–8851.
- 5 D. M. Guldi, I. Zilbermann, G. Anderson, A. Li, D. Balbinot, N. Jux, M. Hatzimarinaki, A. Hirsch and M. Prato, *Chem. Commun.*, 2004, 726–727.
- 6 M. Morisue, S. Yamatsu, N. Haruta and Y. Kobuke, *Chem.–Eur. J.*, 2005, **11**, 5563–5574.
- 7 S. O. Krabbenborg and J. Huskens, *Angew. Chem., Int. Ed.*, 2014, **53**, 9152–9167.
- 8 P. Parkinson, C. E. Knappe, N. Kamonsutthipajit, K. Sirithip, J. D. Matichak, H. L. Anderson and L. M. Herz, *J. Am. Chem. Soc.*, 2014, **136**, 8217–8220.
- 9 H. Hayashi, I. V. Lightcap, M. Tsujimoto, M. Takano, T. Umeyama, P. V. Kamat and H. Imahori, *J. Am. Chem. Soc.*, 2011, **133**, 7684–7687.
- 10 F. Garo and R. Häner, *Angew. Chem., Int. Ed.*, 2012, **51**, 916–919.
- 11 P. M. Beaujuge and J. M. J. Fréchet, *J. Am. Chem. Soc.*, 2011, **133**, 20009–20029.
- 12 T. Aida, E. W. Meijer and S. I. Stupp, *Science*, 2012, **335**, 813–817.
- 13 M. R. Wasielewski, *Acc. Chem. Res.*, 2009, **42**, 1910–1921.
- 14 A. Mishra and P. Bäuerle, *Angew. Chem., Int. Ed.*, 2012, **51**, 2020–2067.
- 15 R. Kumar, J. MacDonald, T. Singh, L. Waddington and A. Holmes, *J. Am. Chem. Soc.*, 2011, **133**, 8564–8573.
- 16 M. Urbani, J. Iehl, I. Osinska, R. Louis, M. Holler and J.-F. Nierengarten, *Eur. J. Org. Chem.*, 2009, 3715–3725.
- 17 Y. Zhang, Y. Matsuo, C.-Z. Li, H. Tanaka and E. Nakamura, *J. Am. Chem. Soc.*, 2011, **133**, 8086–8089.
- 18 D. Bonifazi, O. Enger and F. Diederich, *Chem. Soc. Rev.*, 2007, **36**, 390–414.
- 19 F. D'Souza and O. Ito, *Chem. Commun.*, 2009, 4913–4928.
- 20 S. S. Babu, H. Möhwald and T. Nakanishi, *Chem. Soc. Rev.*, 2010, **39**, 4021–4035.
- 21 F. Giacalone and N. Martín, *Adv. Mater.*, 2010, **22**, 4220–4248.
- 22 N. Sakai, R. Bhosale, D. Emery, J. Mareda and S. Matile, *J. Am. Chem. Soc.*, 2010, **132**, 6923–6925.
- 23 N. Sakai, M. Lista, O. Kel, S.-I. Sakurai, D. Emery, J. Mareda, E. Vauthey and S. Matile, *J. Am. Chem. Soc.*, 2011, **133**, 15224–15227.
- 24 E. Orentas, M. Lista, N.-T. Lin, N. Sakai and S. Matile, *Nat. Chem.*, 2012, **4**, 746–750.
- 25 N. Sakai and S. Matile, *J. Am. Chem. Soc.*, 2011, **133**, 18542–18545.
- 26 A. Bolag, H. Hayashi, P. Charbonnaz, N. Sakai and S. Matile, *ChemistryOpen*, 2013, **2**, 55–57.
- 27 A. Bolag, J. Lopez-Andarias, S. Lascano, S. Soleimanpour, C. Atienza, N. Sakai, N. Martín and S. Matile, *Angew. Chem., Int. Ed.*, 2014, **53**, 4890–4895.
- 28 M. Turbiez, P. Frère, M. Allain, C. Videlot, J. Ackermann and J. Roncali, *Chem.–Eur. J.*, 2005, **11**, 3742–3752.
- 29 P. M. Beaujuge, C. M. Amb and J. R. Reynolds, *Acc. Chem. Res.*, 2010, **43**, 1396–1407.
- 30 X. Guo, J. Quinn, Z. Chen, H. Usta, Y. Zheng, Y. Xia, J. W. Hennek, R. P. Ortiz, T. J. Marks and A. Facchetti, *J. Am. Chem. Soc.*, 2013, **5**, 1986–1996.
- 31 W. Li, H. E. Katz, A. J. Lovinger and J. G. Laquindanum, *Chem. Mater.*, 1999, **11**, 458–465.
- 32 L. J. A. Koster, M. Kemerink, M. M. Wienk, K. Maturová and R. A. J. Janssen, *Adv. Mater.*, 2011, **23**, 1670–1674.
- 33 B. J. Kim, H. Yu, J. K. Oh, M. S. Kang and J. H. Cho, *J. Phys. Chem. C*, 2013, **117**, 10743–10749.
- 34 V. Coropceanu, J. Cornil, D. A. da Silva Filho, Y. Olivier, R. Silbey and J.-L. Bredas, *Chem. Rev.*, 2007, **107**, 926–952.
- 35 N. Sakai, P. Charbonnaz, S. Ward and S. Matile, *J. Am. Chem. Soc.*, 2014, **136**, 5575–5578.
- 36 G. A. H. Wetzelaer, M. Kuik, M. Lenes and P. W. M. Blom, *Appl. Phys. Lett.*, 2011, **99**, 153506.
- 37 J. H. Lee, S. Cho, A. Roy, H.-T. Jung and A. J. Heeger, *Appl. Phys. Lett.*, 2010, **96**, 163303.
- 38 A. Wilson, G. Gasparini and S. Matile, *Chem. Soc. Rev.*, 2014, **43**, 1948–1962.
- 39 J.-M. Lehn, *Top. Curr. Chem.*, 2012, **322**, 1–32.
- 40 J. Li, P. Nowak and S. Otto, *J. Am. Chem. Soc.*, 2013, **135**, 9222–9239.
- 41 S. P. Black, J. K. M. Sanders and A. R. Stefankiewicz, *Chem. Soc. Rev.*, 2014, **43**, 1861–1872.
- 42 M. Lista, J. Areephong, N. Sakai and S. Matile, *J. Am. Chem. Soc.*, 2011, **133**, 15228–15231.

